Simulation of the record Arctic stratospheric ozone depletion in 2020

Jens-Uwe Grooß[1] and Rolf Müller[1]

[1]Forschungszentrum Jülich

November 22, 2022

Abstract

In Arctic winter and spring 2020, the stratospheric temperatures were exceptionally low for a long time period and the polar vortex was very stable. As a consequence, significant ozone depletion occurred in Northern polar regions in spring 2020. Here, we present simulations by the Chemical Lagrangian Model of the Stratosphere (CLaMS) that addresses the development of chlorine compounds and ozone in the polar stratosphere in 2020. The simulation is able to reproduce relevant observations which is shown by comparisons with MLS, ACE-FTS and OMI data. Although the concentration of chlorine and bromine compounds in the polar stratosphere has decreased by more than 10% compared to the peak values around the year 2000, the meteorological conditions in winter and spring 2020 caused an unprecedented ozone depletion. The simulated lowest ozone mixing ratio was around 0.05 ppmv and the ozone depletion in the vortex core in the lower stratosphere reached 133 Dobson Units, which is more than the loss in the years 2011 and 2016 that had the largest Arctic ozone depletion so far.

Simulation of the record Arctic stratospheric ozone depletion in 2020

Jens-Uwe Grooß[1] and Rolf Müller[1]

[1]Institut für Energie- und Klimaforschung – Stratosphäre (IEK-7), Forschungszentrum Jülich, Germany

submitted to J. Geophys. Res. on June 19, 2020

Key Points:

- cold and stable vortex in Arctic winter 2019/2020
- observation of significant ozone loss
- simulations reproduce observed ozone loss

Corresponding author: Jens-Uwe Grooß, `j.-u.grooss@fz-juelich.de`

Abstract

In Arctic winter and spring 2020, the stratospheric temperatures were exceptionally low for a long time period and the polar vortex was very stable. As a consequence, significant ozone depletion occurred in Northern polar regions in spring 2020. Here, we present simulations by the Chemical Lagrangian Model of the Stratosphere (CLaMS) that addresses the development of chlorine compounds and ozone in the polar stratosphere in 2020. The simulation is able to reproduce relevant observations which is shown by comparisons with MLS, ACE-FTS and OMI data. Although the concentration of chlorine and bromine compounds in the polar stratosphere has decreased by more than 10% compared to the peak values around the year 2000, the meteorological conditions in winter and spring 2020 caused an unprecedented ozone depletion. The simulated lowest ozone mixing ratio was around 0.05 ppmv and the ozone depletion in the vortex core in the lower stratosphere reached 133 Dobson Units, which is more than the loss in the years 2011 and 2016 that had the largest Arctic ozone depletion so far.

1 Introduction

It is well established that the Antarctic ozone hole (Farman et al., 1985; Jones & Shanklin, 1995) is caused by chemical ozone depletion in spring through catalytic cycles driven by chlorine and bromine compounds (e.g., Canty et al., 2016; WMO, 2019). For these cycles to run efficiently, chlorine needs to be activated from the so called reservoir compounds HCl and $ClONO_2$ by heterogeneous reactions. These heterogeneous reactions take place only at low temperatures present typically in polar winter and spring; these reactions occur on the surfaces of Polar Stratospheric Clouds (PSCs) and on cold sulfate aerosol (Solomon, 1999; Drdla & Müller, 2012).

The reason for an enhanced stratospheric chlorine and bromine loading, commonly referred to as Equivalent Effective Stratospheric Chlorine (EESC) is chlorine and bromine released from anthropogenically emitted CFCs and halons (Newman et al., 2007; Engel et al., 2018). Because of the regulations of the Montreal protocol and its amendments and adjustments, the stratospheric halogen loading peaked around the year 2000. Due to the long atmospheric lifetime of the CFCs and halons, the EESC (polar winter conditions) is currently reduced by about 11-12% of the peak value in the year 2002 (Newman et al., 2007; Engel et al., 2018; WMO, 2019). This level corresponds to the EESC of about the year 1992. In addition to the long-term decline of EESC in the atmosphere, there is also an inter-annual variability of inorganic chlorine (Cl_y, i.e. the sum of the destruction products of anthropogenically emitted CFCs) in the polar stratosphere, which is caused by the inter-annual variability of descent in the polar vortex (Strahan et al., 2014). In Antarctica, the expected decline of Cl_y is about 20 pptv/y, whereas the year-to-year variability ranges from -200 to $+150$ pptv (Strahan et al., 2014); this effect will be present in the Arctic as well and points to the importance of an accurate representation of diabatic descent in studies of polar ozone loss.

Strong chemical polar ozone loss in the stratosphere has been identified in cold Arctic polar winters and springs exhibiting a persistent polar vortex into late winter and early spring e.g., in March 1997, 2011, and 2016 (Newman et al., 1997; Müller, Crutzen, et al., 1997; Müller, Grooß, et al., 1997; Tilmes et al., 2004; Weber et al., 2011; G. L. Manney et al., 2011; Grooß et al., 2014; Pommereau et al., 2018). However, stratospheric temperatures in the Arctic in winter and spring are generally much higher than in the Antarctic. However, there are reported cases, where chlorine activation occurs in association with the formation of PSCs over only a small portion of the vortex, but this small cold portion nonetheless resulted is a substantial activation vortex wide (Wegner et al., 2016). Because of a higher dynamic activity in the Arctic, which results in a lower stability and in higher temperatures of the Arctic polar vortex, Arctic ozone depletion is typically much

less pronounced and much more variable than in the Antarctic (WMO, 2019; Bernhard et al., 2020).

Despite decreasing halogen levels in the stratosphere (Newman et al., 2007; Engel et al., 2018), the lower and more variable stratospheric temperatures may cause larger areas to be perceptible for heterogeneous chemistry and chlorine activation, resulting in ozone depletion, especially in years with a stable polar vortex extending into spring. Rex et al. (2006) put forward the hypothesis that cold Arctic stratospheric winters tend to get colder, resulting in an increasingly strong ozone loss. There is a debate on the accuracy of such projections based on studies using extreme value statistics (Rieder & Polvani, 2013) or sunlit vortex volumes (Pommereau et al., 2013). Detailed studies of re-analyses and homogenized radiosonde data (Bohlinger et al., 2014) confirm a cooling of –0.41 K/decade over the past 3 decades in Arctic spring that fosters ozone depletion, but also an increase of planetary wave activity that disturbs the stability of the polar vortex, which is not favourable for chemical ozone loss. However, in different models participating in the Chemistry-Climate Model Initiative (CCMI), there is no statistically significant change in the frequency of major mid-winter stratospheric sudden warmings (SSWs), the largest instance of wintertime variability in the Arctic stratosphere (Ayarzagüena et al., 2018). Rieder et al. (2014) show that the temperature decrease in the lower stratosphere is dominated by ozone depleting substances as opposed to well-mixed greenhouse gases that dominate the temperature trend in the upper stratosphere. In the Arctic, the role of dynamical processes for determining springtime ozone will likely increase in the future, because of the effect of declining ODSs and rising greenhouse gases. There are Chemistry Climate Model (CCM) simulations that show that even after 2040, when EESC has substantially declined, early springtime Arctic total column ozone in particular years can drop by about 50 to 100 DU below the long-term average (Langematz et al., 2014; Bednarz et al., 2016).

Even in cold Arctic winters, ozone mixing ratios at the end of the ozone depletion period are commonly much higher than in the Antarctic, which has implications for chlorine recovery. In the Antarctic, for very low ozone mixing ratios, chlorine recovery is largely into HCl, whereas in the Arctic, for higher ozone mixing ratios, chlorine recovery is largely into $ClONO_2$ (Crutzen et al., 1992; Müller et al., 1994; Douglass et al., 1995; Grooß et al., 1997). For the chlorine recovery into HCl in the Antarctic, the occurrence of extremely low ozone mixing ratios in the vortex is essential (Grooß et al., 2011; Müller et al., 2018).

Moreover, a strong Arctic polar vortex leads to a reduced poleward transport of ozone, contributing further to low total column ozone values in spring. There have been warm Arctic years in which no chlorine-catalyzed ozone depletion was detected and cold years with a stable vortex that experienced significant ozone depletion (e.g., Tilmes et al., 2006; Müller et al., 2008; Bernhard et al., 2020).

Although the main aspects of polar chlorine activation and the resulting catalytic ozone loss are established (WMO, 2019), some scientific questions in this area remain that have not yet been resolved. In particular, there is observed HCl depletion in the dark polar vortex which cannot be reproduced given the processes currently implemented in models (Grooß et al., 2018).

Here we report on the Arctic ozone depletion in the year 2020 that is unprecedented (Bernhard et al., 2020; G. Manney et al., 2020). The chemical composition observed by satellite instruments is compared with the simulations by the Chemical Lagrangian Model of the Stratosphere (CLaMS). The major causes of the reported severe ozone depletion in the Arctic in 2020 are the low stratospheric temperatures and the exceptionally stable polar vortex extending into spring (Lawrence et al., 2020).

2 Data description

2.1 AURA-MLS

The observations by the Microwave Limb Sounder (MLS) on board the AURA satellite are the main data set used in this study. Further details of the MLS measurements in the Arctic winter 2019/2020 are reported by G. Manney et al. (2020). MLS observes in limb viewing geometry on the so-called A-train orbit, circling the earth 15 times daily covering latitudes from 82°S to 82°N. We use the MLS version 4.2 data (Livesey et al., 2017). Here observations of O_3, N_2O, HCl, H_2O, and HNO_3 are used for model initialisation, boundary conditions and for comparison with the model results.

2.2 ACE-FTS

The experiment ACE-FTS on the satellite SCISAT is a Fourier Transform Spectrometer (FTS) with high spectral resolution ($0.02\,\mathrm{cm}^{-1}$) operating from 2.2 to 13.3 μm wavelength employing a Michelson interferometer (Bernath et al., 2005). Since 2004, it observes around 30 profiles per day in solar occultation geometry with the majority of the measurements being in high latitudes. Here we use version 3.6 data of O_3, N_2O, as well as the five main components of total inorganic nitrogen NO_y (NO, NO_2, N_2O_5, HNO_3, $ClONO_2$).

2.3 AURA-OMI

The Ozone Monitoring Instrument (OMI) onboard the the satellite AURA is a limb viewing spectrometer that measures the solar radiation back-scattered by the Earth's atmosphere and surface over the entire UV/VIS wavelength range from 270 to 500 nm (Levelt et al., 2006). It is in the succession of previous Total Ozone Monitoring Spectrometers (TOMS). Since 2004, OMI provided measurements in global coverage of the distribution of atmospheric ozone column on a daily basis.

3 Model description

3.1 Model setup

The simulations described here have been performed with the Chemical Lagrangian Model of the Stratosphere (CLaMS). Unlike in previous publications, the chemical transport model CLaMS is driven here by operational analyses by the European Centre of Medium Range Weather Forecasts (ECMWF), as neither re-analyses ERA-Interim nor ERA-5 were available when the simulations were performed. Thus the vertical velocities were derived from heating rates calculated by an offline radiation module based on the Morcrette scheme as in an earlier model setup (Morcrette, 1991; Zhong & Haigh, 1995; Konopka et al., 2004). The vertical model coordinate is the hybrid potential temperature ζ (Konopka et al., 2004; Pommrich et al., 2014) that is identical to potential temperature above 100 hPa and corresponds to pressure levels below with a smooth transition. The model simulation described here starts on 1 November 2019 and runs until mid-April. The model domain consists of the Northern hemisphere with a horizontal resolution of 100 km. The vertical range is from the surface to 900 K potential temperature divided into 32 levels with a variable resolution in the stratosphere ranging from 0.7 km at 9-12 km to 1 km at the top layer yielding about 820.000 air parcels in total.

The chemical scheme used here is the same as described earlier (McKenna et al., 2002; Grooß et al., 2011, 2018). In particular, a comprehensive stratospheric chemistry scheme is employed which includes a full set of heterogeneous reactions. The vertical redistribution of NO_y and H_2O due to sedimenting NAT and ice particles is determined by Lagrangian NAT and ice particle tracking (Grooß et al., 2018; Tritscher et al., 2019).

This algorithm allows denitrification to be represented in the model and also dehydration, albeit to a smaller extent in the shown simulation.

3.2 Initialisation and boundary conditions

Both the chemical composition at the begin of the simulation and the boundary conditions at the surface and the top model layer at 900 K potential temperature are derived from a variety of data and model results. This is similar to previous work (Grooß et al., 2014). Data from the Microwave Limb Sounder (MLS) within ±2.5 days of the initial time for O_3, HNO_3, H_2O, HCl and N_2O have been used. The observation locations have been transferred to the initial time using CLaMS trajectories and averaged to a 2° latitude × 6° longitude grid. In the troposphere below 350 K potential temperature the initialisation of these compounds is taken from a multi-annual CLaMS simulation with simplified chemistry setup (Pommrich et al., 2014). For total inorganic nitrogen (NO_y), chlorine (Cl_y) and bromine (Br_y), tracer correlations with N_2O have been used. NO_y was derived from ACE-FTS from the sum of the observations of HNO_3, NO, NO_2, N_2O_5 and $ClONO_2$ on 1 October to 21 November 2019 in different latitude bands that correlate well with N_2O. Inorganic chlorine (Cl_y) and bromine compounds (Br_y) were initialized using correlations with N_2O derived from balloon observations (Grooß et al., 2018). The partitioning within these chemical families has been taken from a 2-D reference model (Grooß, 1996) with updated boundary conditions (WMO, 2019).

The chemical composition at the upper boundary at the 900 K potential temperature level was calculated using the same data sources. Twice per month, the data as described above at this level are mapped and averaged into bins of equivalent latitude (Lary et al., 1995). From that, the chemical composition at the upper boundary is determined. Simulations with this setup had been performed for Arctic winters since 2010.

4 Results

The CLaMS simulation aims to reproduce the processes involved in the Arctic stratospheric ozone depletion over the winter 2019/2020. In the simulation, the formation of NAT particles starts already on 16 November 2019. We analyze the observations and the model results in the polar vortex using the concept of equivalent latitude Φ_e (Lary et al., 1995). The resulting chlorine activation is exceptionally long. (ClO_x/Cl_y) averaged over the polar vortex core (Φ_e>75°N) increases above 50% rather early on 14 December between about 490 K and 540 K potential temperature. Therefore some ozone depletion occurred already in December. Chlorine activation in 2020 lasts until 22 March, and the polar vortex remains still stable into the month of April (Lawrence et al., 2020).

4.1 Descent in the polar vortex

For validation of the simulation results, it is essential to demonstrate the ability of the model to reproduce atmospheric observations. One important aspect of the simulation is whether the transport and dynamics is represented correctly. Especially the diabatic descent of air inside the polar vortex should be realistic. Diabatic descent in a particular winter determines the ozone mixing ratios at a given potential temperature level in spring, but also the the available Cl_y (Strahan et al., 2014). Thus we investigated whether the descent of vortex air is simulated properly. Figure 1 shows a comparison of N_2O profiles in the vortex core observed by ACE-FTS between 23 and 29 March in the vortex (Φ_e>70°N) and the corresponding CLaMS data evaluated at the observation locations. The solid lines show the mean mixing ratio profile and the dotted lines show the standard deviation. The CLaMS simulation shows a slightly lower descent than observed between early November and late March, for 200 ppbv N_2O corresponding to a change of 54 K instead of 64 K in potential temperature. For 100 ppbv N_2O the simulated de-

scent is 68 K instead of the observed 90 K. This difference of vertical displacements is important, but is in the order of the vertical model resolution.

4.2 Ozone depletion

The focus of this study is on the simulation of ozone depletion in the Arctic in 2020. First, the overall development of ozone is compared with MLS observations. As MLS measures about 3500 profiles per day, the comparison is done in a way that similar air-masses are averaged. For that, both the data and the simulations are averaged daily into equivalent latitude and potential temperature bins. The width of the equivalent latitude bins is chosen such that they correspond to equal geographical areas. Figure 2 displays different illustrations of these averages. Panel a shows the time development of the vortex core average profiles for equivalent latitudes Φ_e>75°N, panel b shows the time development of the mixing ratio at the 450 K potential temperature level as a function of equivalent latitude. Panels c and d show this average for two chosen dates, 31 January and 25 March respectively. Figure 3 shows the corresponding development of ozone derived from the CLaMS simulation. Although there are some small differences, the ozone depletion over winter and spring is well reproduced by the simulation. The strongest effect of the ozone depletion is seen between 400 K and 500 K potential temperature towards the end of March. The gradients of ozone at the edge of the polar vortex are reproduced well. On 27 March, the mean MLS ozone mixing ratio (±standard deviation) on the 450 K level for equivalent latitudes above 75°N is 0.21±0.25 ppmv. The corresponding ozone mixing ratio from the CLaMS simulation is 0.29±0.26 ppmv.

Figure 4 shows the chemical ozone change that is calculated as the difference between the simulated ozone and a passive ozone tracer that has identical initialisation and boundary conditions and transport, but no chemical change. The maximum ozone depletion in the vortex core average (Φ_e>75°N) is 2.74 ppmv reached on 30 March on the 470 K potential temperature level. After that day this value remained constant until mid-April indicating no additional ozone loss but also no significant mixing with mid-latitude ozone-rich air.

Also visible is an ozone depletion in mid-latitudes in the middle stratosphere between 600 K and 700 K. This ozone depletion is dominated by NO_x-induced catalytic cycles, but this topic is not further considered here.

With respect to the variability of surface UV radiation, the total ozone column is important. To calculate the model total ozone column, the ozone column above 900 K potential temperature needed to be added to the column over vertical model domain. The column above 900 K amounts to about 30 DU as determined from a climatology depending on equivalent latitude and time of year (Grooß & Russell, 2005). The geographical distribution of ozone columns is also well reproduced by the simulation. Figure 5 shows the comparison of the geographical distribution of ozone columns from AURA-OMI and CLaMS for March 29. Note that the OMI data are observed and accumulated over a 24-h period (resulting in a discontinuity on the date line) while the model data are displayed for the synoptic time 12:00 UTC. This comparison shows the ability of the CLaMS simulation to reproduce the gradients in the ozone distribution accurately.

Figure 6 shows the average development of the simulated ozone column depletion within the vortex (Φ_e>70°N) between 350 ans 600 K potential temperature. For this volume the maximum ozone depletion of 133 DU has been reached on 25 March. For comparison, we also show this quantity for comparable CLaMS simulations for the years with significant Arctic ozone depletion in the previous decade including 2011 and 2016. The calculated column ozone depletion in 2020 clearly exceeds the depletion in 2011 and 2016.

The simulated ozone profiles were also compared with observations. Figure 7 shows the average vortex core ozone profile observed by ACE-FTS for the time between 23 and

29 March. The corresponding CLaMS simulations were evaluated at the ACE-FTS tangent point locations. Dotted lines show the standard deviation within these profiles. Around 450 K potential temperature, the simulations show lower ozone mixing ratios but within the standard deviation. This could possibly be cause by the fact that the ACE-FTS occultation retrieval are also influenced by larger ozone concentrations at higher levels along the viewing beam.

The simulated ozone mixing ratios did not quite reach the low levels reported for the Antarctic ozone hole (Solomon et al., 2005). Grooß et al. (2011) showed that in the Antarctic ozone hole, the chemical ozone depletion can continue until very low ozone mixing ratios of the order of 10 ppbv have been reached. Before the minimum ozone mixing ratios are reached, chlorine activation is maintained even though there is a considerable speed up of the reaction of Cl with CH_4 (Douglass et al., 1995; Grooß et al., 2011; Müller et al., 2018) caused by decreasing ozone mixing ratios themselves. However, this chlorine deactivation reaction is first balanced by immediate heterogeneous chlorine activation. If this balance terminates, it is possible that practically all available inorganic chlorine species are converted to HCl at a time when PSCs are still available (Müller et al., 2018). For typical Arctic ozone mixing ratios, the dominant fraction of the active chlorine species undergo deactivation into $ClONO_2$ by the reaction $ClO+NO_2$ (Müller et al., 1994; Douglass et al., 1995).

The development of individual air masses with very low ozone mixing ratios cannot be well simulated, if mixing or diffusion is over-estimated in a numerical model. Here we employ Lagrangian simulations which have an advantage as they follow individual air masses for some time without mixing. Also, Lagrangian simulations did reflect the low Antarctic ozone mixing ratios (Grooß et al., 2011). In the current simulation, the lowest simulated ozone mixing ratio in the polar lower stratosphere of 48.5 ppbv was reached on March 24 (84°N, 131°E, θ=439 K). This individual air parcel was not affected by the mixing algorithm for 50 days. Figure 8 shows the temporal development of ozone and chlorine compounds of this air parcel. For an extended period, from about mid February to early March ClO_x levels remain strongly elevated in this air parcel, while the mixing ratios of HCl, $ClONO_2$, and HOCl remain very low. The NAT equilibrium temperature T_{NAT} is shown in the top panel calculated using simulated HNO_3 and H_2O. Changes in T_{NAT} are due to local denitrification and nitrification by the sedimenting NAT particles. Also shown is the threshold temperature for chlorine activation on liquid aerosols T_{ACL} as defined by Drdla and Müller (2012) that does not depend on HNO_3. There is no deactivation occurring during until early March, neither into $ClONO_2$, nor into HCl. Starting in early March, similar as in the Antarctic (e.g., Grooß et al., 1997), the air parcel experiences a complete deactivation into HCl with temperatures partly below T_{NAT}, albeit on a longer time scale of about 2 weeks. The exact location of the simulated lowest ozone mixing ratio is not relevant and it is very sensitive on the ozone initialisation cannot be done with an accuracy of a few ppbv. Also with respect to denitrification and T_{NAT}, the model results are unlikely to represent the precise day-to-day variability a at specific location. But on a larger vortex scale, they should be representative. The vortex core average HCl and $ClONO_2$ (Φ_e>70°N) at 500 K potential temperature are shown in Fig. 9a together with the corresponding MLS HCl data. The rate of increase of HCl mixing ratios in late March is similar suggesting also similar low ozone mixing ratios.

Figure 9 indicates a discrepancy in HCl during the onset of chlorine activation. Grooß et al. (2018) showed that there is a yet unexplained discrepancy in HCl between simulations and observations. In the cold dark polar vortex core in early winter stratosphere the observed depletion of HCl is faster than simulated. This effect is most pronounced in the Southern hemisphere, but has been also seen in the 2016 Arctic winter. It is also seen here for the year 2020, but to a lesser extent than in the simulation for the winter 2015/2016 (Grooß et al., 2018). This is probably due to the earlier onset of chlorine activation in 2019/2020 when still more sunlight was available.

5 Conclusions

The Arctic winter 2019/2020 was exceptionally cold in the polar stratosphere and the polar vortex was stable for a long time with the consequence of significant ozone depletion. This has been shown by CLaMS simulations that correspond well to the observations. Even though the stratospheric halogen loading (EESC) has decreased since its peak in 2000 by about 11-12%, these meteorological conditions cause an Arctic ozone depletion that has been unprecedented. The calculated vortex average ozone column depletion between 350 and 600 K potential temperature was 133 DU in late March. On the 470 K level in the vortex core the ozone mixing ratio was depleted by 2.74 ppmv on 30 March. The lowest simulated ozone mixing ratio in the lower stratosphere was about 50 ppbv. If the temperature trend in the lower polar stratosphere continues, more Arctic winters with similar ozone depletion are possible even though the chlorine loading is decreasing.

Acknowledgments

The authors gratefully acknowledge the computing time for the CLaMS simulations granted on the supercomputer JURECA at Jülich Supercomputing Centre (JSC) under the VSR project ID JICG11. This paper is based on the model CLaMS which has been developed and maintained by a comprehensive team including Nicole Thomas, Gebhard Günther, Paul Konopka, Felix Plöger, and Ines Tritscher. We thank Gloria Manney, Michelle Santee and the MLS team, Peter Bernath and Kaley Walker and the ACE-FTS team as well as the OMI team for the enormous work on providing their high quality data sets.

The satellite data used in this study are publicly available. MLS level 2 data (version 4) were obtained from https://acdisc.gesdisc.eosdis.nasa.gov/data/Aura_MLS_Level2, OMI level 3 data from https://ozonewatch.gsfc.nasa.gov/data/omi and ACE-FTS data (version 3.6) from https://databace.scisat.ca/level2/ace_v3.5_v3.6 . CLaMS model results in the equivalent latitude/potential temperature averages are available from https://datapub.fz-juelich.de/slcs/clams/ozoneloss_2020 .

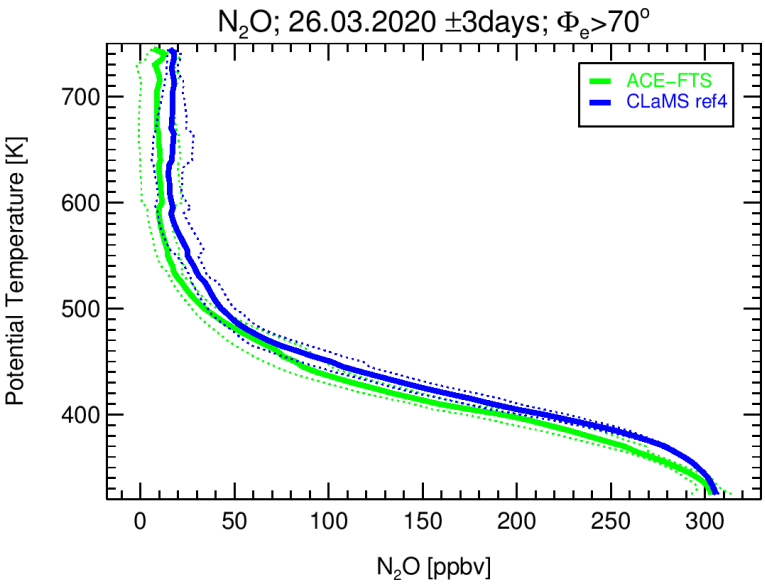

Figure 1. ACE-FTS comparison: vortex (Φ_e>70°N) N_2O mixing ratios in the time frame 26 March ±3 days. The green line shows the average N_2O mixing ratio profile. Dotted lines correspond to the standard deviation of the measurements ($\pm 1\sigma$). Blue lines are from the CLaMS simulation interpolated to ACE-FTS profile locations evaluated correspondingly.

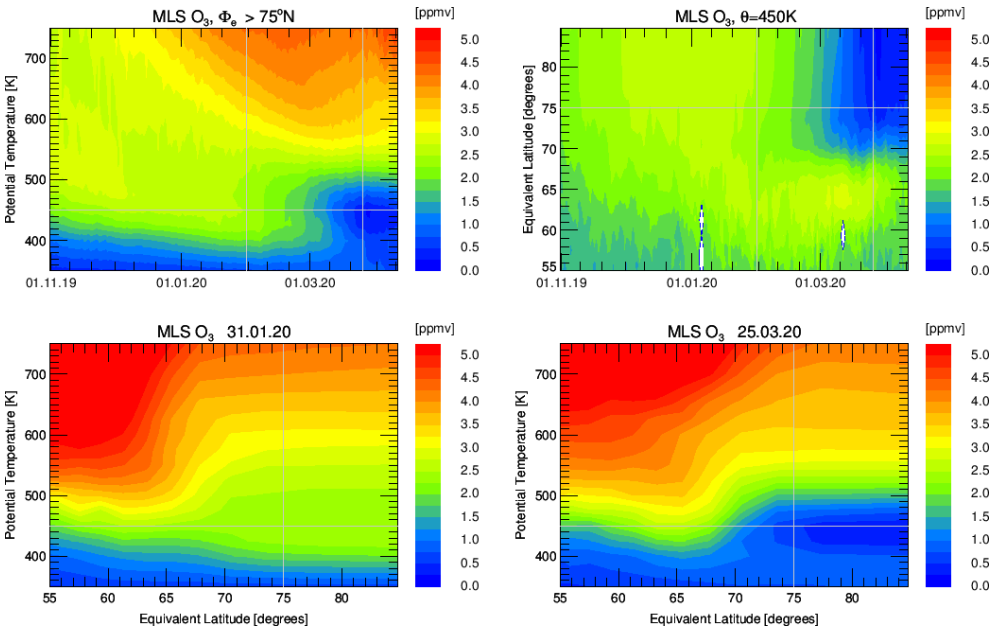

Figure 2. MLS ozone observations averaged in equivalent latitude/potential temperature space. The top left panel shows the vortex (Φ_e>70°N) average as a function of potential temperature and time. The top right panel shows the observations on the 450 K potential temperature levels as function of equivalent latitude and time and the lower panels show these data for two chosen days, 31 January and 29 March.

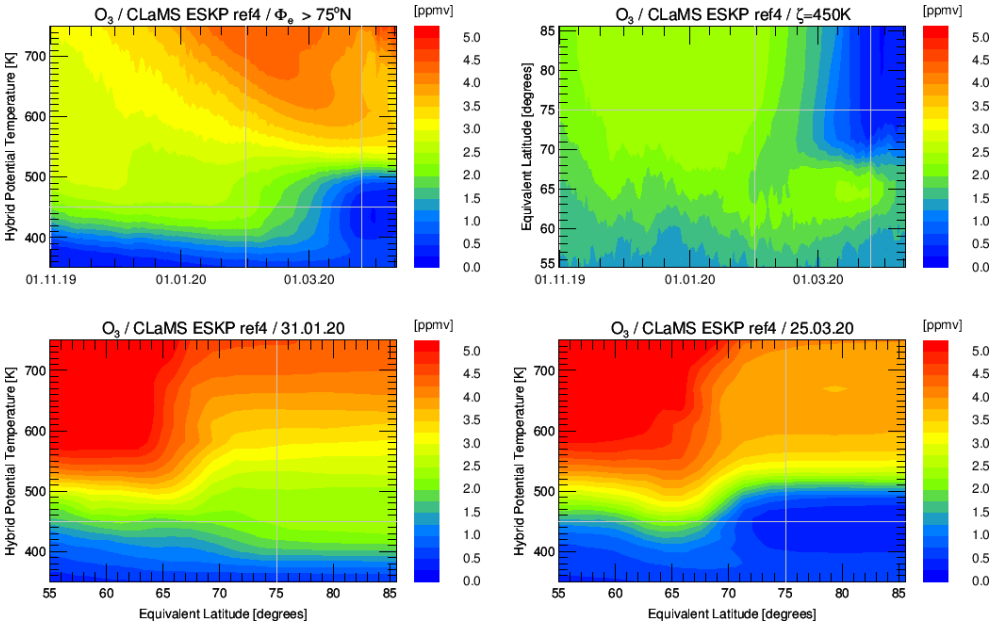

Figure 3. CLaMS simulation of ozone plotted corresponding to Figure 2.

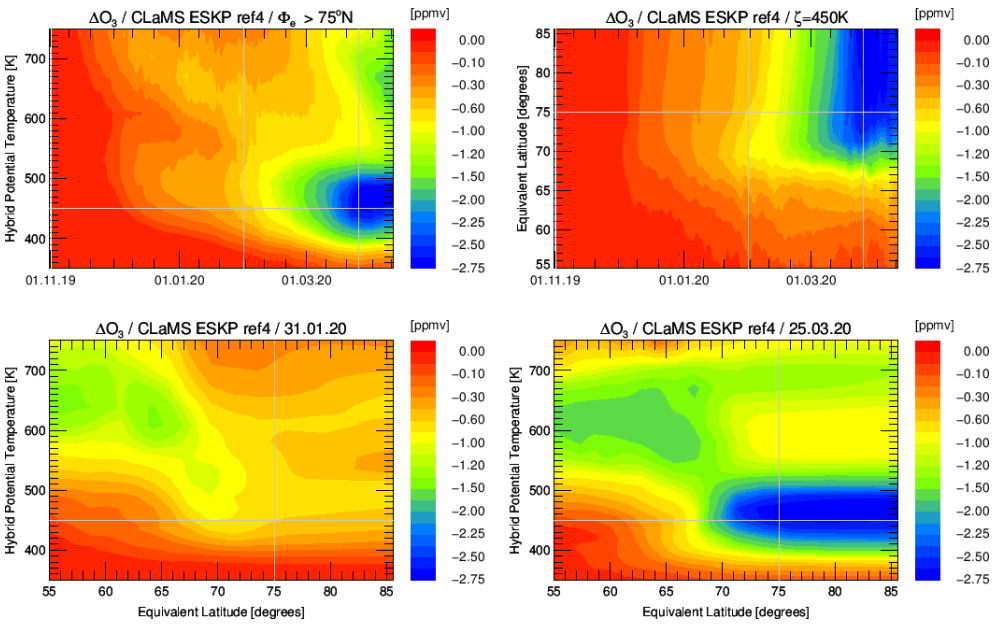

Figure 4. Simulated chemical ozone depletion determined by the difference of simulated ozone and the passive ozone tracer corresponding to Figures 2 and 3.

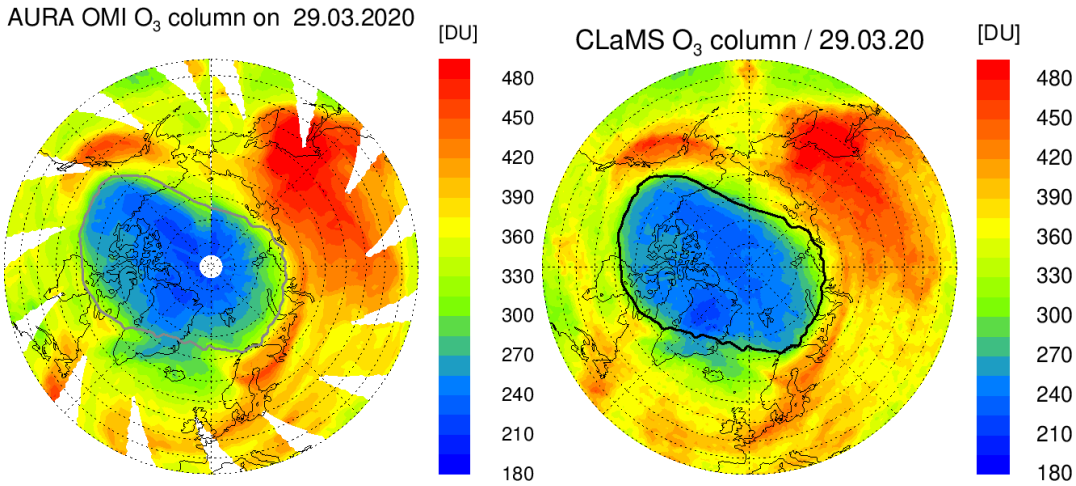

Figure 5. Ozone columns for 29 March (a) from AURA-OMI and (b) from the CLaMS simulation. Ozone column above 900 K in CLaMS plot is taken from the HALOE-climatology (Grooß & Russell, 2005). The solid line marks the vortex edge after Nash et al. (1996) on the 450 K potential temperature level.

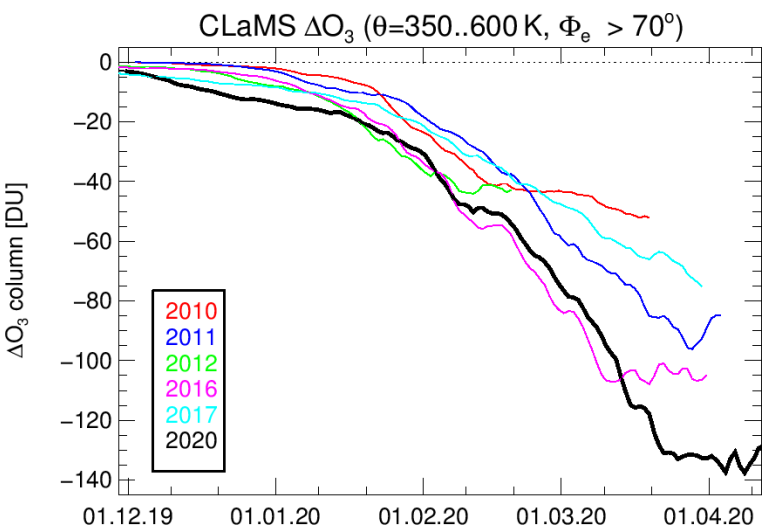

Figure 6. Development of simulated ozone column depletion between 350 and 600 K potential temperature. For comparison, also comparable simulations for other years of significant Arctic ozone depletion including 2011 and 2016 are shown. The maximum column ozone depletion on 2020 is 133 DU at 25 March.

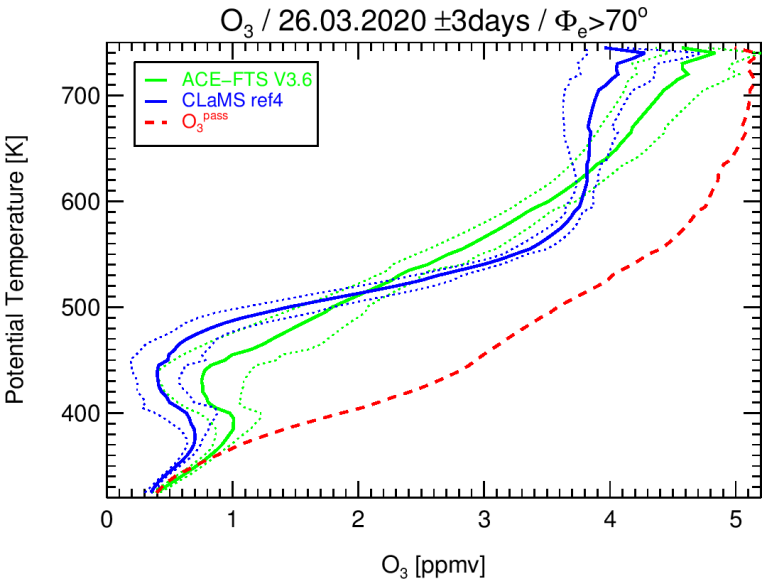

Figure 7. ACE-FTS comparison: vortex (Φ_e>70°N) ozone mixing ratios in the time frame 26 March ±3 days. The green line shows the average ACE-FTS ozone mixing ratio profile. Dotted lines correspond to the standard deviation of the measurements ($\pm 1\sigma$). Blue lines are from the CLaMS simulation interpolated to ACE-FTS profile locations evaluated correspondingly. The red dashed line marks the mixing ratio of the passive ozone tracer.

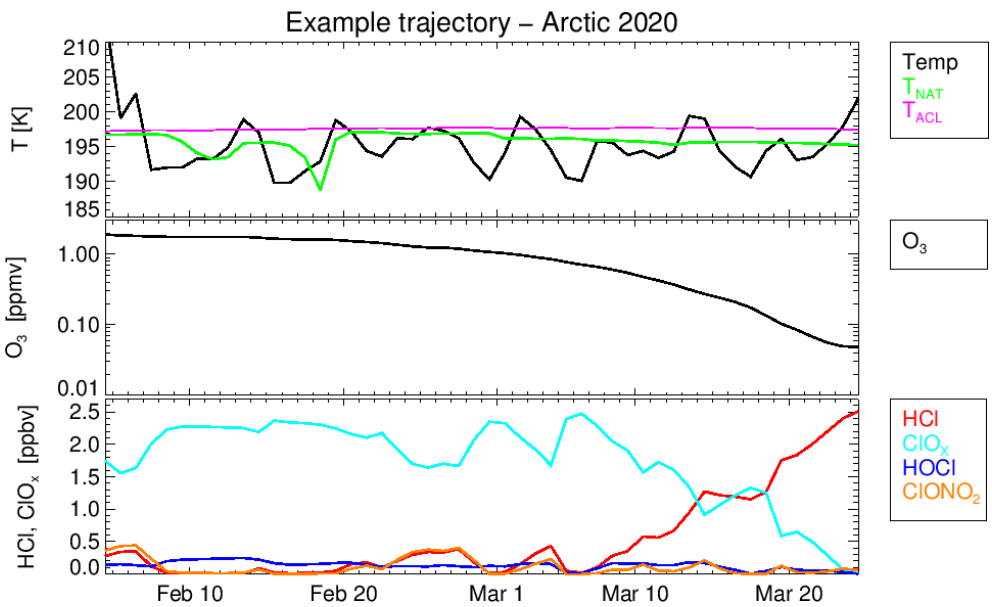

Figure 8. 50-day development of one example air parcel trajectory from the CLaMS simulation that is not affected by mixing over the shown time period. The top panel shows the temperature, the NAT equilibrium temperature T_{NAT} as well as the threshold temperature for chlorine activation on liquid aerosols T_{ACL} after Drdla and Müller (2012). The mixing ratio of ozone (middle, logarithmic ordinate) and chlorine compounds HCl, $ClONO_2$, ClO_x (=$ClO+2\times Cl_2O_2$, $2\times Cl_2$) and HOCl (bottom) are shown. The ozone mixing ratio on 24 March (84°N, 131°E, θ=439 K) is 48.5 ppbv.

References

Ayarzagüena, B., Polvani, L. M., Langematz, U., Akiyoshi, H., Bekki, S., Butchart, N., ... Zeng, G. (2018). No robust evidence of future changes in major stratospheric sudden warmings: a multi-model assessment from ccmi. *Atmos. Chem. Phys.*, *18*(15), 11277–11287. doi: 10.5194/acp-18-11277-2018

Bednarz, E. M., Maycock, A. C., Abraham, N. L., Braesicke, P., Dessens, O., & Pyle, J. A. (2016). Future arctic ozone recovery: the importance of chemistry and dynamics. *Atmos. Chem. Phys.*, *16*, 12159-12176. doi: 10.5194/acp-16-12159-2016

Bernath, P. F., McElroy, C. T., Abrams, M. C., Boone, C. D., Butler, M., Camy-Peyret, C., ... Zou, J. (2005). Atmospheric Chemistry Experiment (ACE) Mission overview. *Geophys. Res. Lett.*, *32*(15). doi: 10.1029/2005GL022386

Bernhard, G. H., Fioletov, V. E., Grooß, J.-U., Ialongo, I., Johnsen, B., Lakkala, K., ... Svendby, T. (2020). Record-Breaking Increases in Arctic Solar Ultraviolet Radiation Caused by Exceptionally Large Ozone Depletion in 2020. *Geophys. Res. Lett.*. (in preparation)

Bohlinger, P., Sinnhuber, B.-M., Ruhnke, R., & Kirner, O. (2014). Radiative and dynamical contributions to past and future arctic stratospheric temperature trends. *Atmos. Chem. Phys.*, *14*, 1679–1688. doi: 10.5194/acp-14-1679-2014

Canty, T. P., Salawitch, R. J., & Wilmouth, D. M. (2016). The kinetics of the ClOOCl catalytic cycle. *J. Geophys. Res.*, *121*(22), 13768-13783. doi: 10.1002/2016JD025710

Crutzen, P. J., Müller, R., Brühl, C., & Peter, T. (1992). On the potential importance of the gas phase reaction $CH_3O_2 + ClO \rightarrow ClOO + CH_3O$ and the heterogeneous reaction $HOCl + HCl \rightarrow H_2O + Cl_2$ in "ozone hole" chemistry. *Geophys. Res. Lett.*, *19*(11), 1113-1116. doi: 10.1029/92GL01172

Douglass, A. R., Schoeberl, M. R., Stolarski, R. S., Waters, J. W., Russell III, J. M., Roche, A. E., & Massie, S. T. (1995). Interhemispheric differences in springtime production of HCl and $ClONO_2$ in the polar vortices. *J. Geophys. Res.*, *100*, 13967-13978.

Drdla, K., & Müller, R. (2012). Temperature thresholds for chlorine activation and ozone loss in the polar stratosphere. *Ann. Geophys.*, *30*, 1055-1073. doi: 10.5194/angeo-30-1055-2012

Engel, A., Bönisch, H., Ostermöller, J., Chipperfield, M. P., Dhomse, S., & Jöckel, P. (2018). A refined method for calculating equivalent effective stratospheric chlorine. *Atmos. Chem. Phys.*, *18*(2), 601–619. doi: 10.5194/acp-18-601-2018

Farman, J. C., Gardiner, B. G., & Shanklin, J. D. (1985). Large losses of total ozone in Antarctica reveal seasonal ClO_x/NO_x interaction. *Nature*, *315*, 207-210.

Grooß, J.-U. (1996). *Modelling of stratospheric chemistry based on HALOE/UARS satellite data* (PhD thesis). University of Mainz.

Grooß, J.-U., Brautzsch, K., Pommrich, R., Solomon, S., & Müller, R. (2011). Stratospheric ozone chemistry in the Antarctic: What controls the lowest values that can be reached and their recovery? *Atmos. Chem. Phys.*, *11*, 12217–12226.

Grooß, J.-U., Engel, I., Borrmann, S., Frey, W., Günther, G., Hoyle, C. R., ... Müller, R. (2014). Nitric acid trihydrate nucleation and denitrification in the arctic stratosphere. *Atmos. Chem. Phys.*, *14*(2), 1055–1073. doi: 10.5194/acp-14-1055-2014

Grooß, J.-U., Müller, R., Spang, R., Tritscher, I., Wegner, T., Chipperfield, M. P., ... Madronich, S. (2018). On the discrepancy of hcl processing in the core of the wintertime polar vortices. *Atmos. Chem. Phys.*, 8647–8666. doi: 10.5194/acp-18-8647-2018

Grooß, J.-U., Pierce, R. B., Crutzen, P. J., Grose, W. L., & Russell III, J. M. (1997). Re-formation of chlorine reservoirs in southern hemisphere polar spring. *J. Geophys. Res.*, *102*, 13141-13152. doi: 10.1029/96JD03505

Grooß, J.-U., & Russell, J. M. (2005). Technical note: A stratospheric climatology for O_3, H_2O, CH_4, NO_x, HCl, and HF derived from HALOE measurements. *Atmos. Chem. Phys.*, *5*, 2797-2807.

Jones, A. E., & Shanklin, J. D. (1995). Continued decline of total ozone over Halley, Antarctica, since 1985. *Nature*, *376*, 409-411.

Konopka, P., Steinhorst, H.-M., Grooß, J.-U., Günther, G., Müller, R., Elkins, J. W., ... McKenna, D. S. (2004). Mixing and ozone loss in the 1999-2000 Arctic vortex: Simulations with the 3-dimensional Chemical Lagrangian Model of the Stratosphere (CLaMS). *J. Geophys. Res.*, *109*. doi: 10.1029/2003JD003792

Langematz, U., Meul, S., Grunow, K., Romanowsky, E., Oberländer, S., Abalichin, J., & Kubin, A. (2014). Future arctic temperature and ozone: The role of stratospheric composition changes. *J. Geophys. Res.*, *119*(5), 2092–2112. Retrieved from `http://dx.doi.org/10.1002/2013JD021100` (2013JD021100) doi: 10.1002/2013JD021100

Lary, D. J., Chipperfield, M. P., Pyle, J. A., Norton, W. A., & Riishøjgaard, L. P. (1995). Three-dimensional tracer initialization and general diagnostics using equivalent PV latitude-potential-temperature coordinates. *Q. J. R. Meteorol. Soc.*, *121*, 187-210.

Lawrence, Z., Perlwitz, J., Butler, A. H., Manney, G. L., Newman, P. A., Lee, S. H., & Nash, E. R. (2020). The Remarkably Strong Arctic Stratospheric Polar Vortex of Winter 2020: Links to Record-Breaking Arctic Oscillation and Ozone Loss. *J. Geophys. Res.*. (submitted)

Levelt, P. F., Van den Oord, G. H. J., Dobber, M. R., Malkki, A., Visser, H., de Vries, J., ... Saari, H. (2006). The ozone monitoring instrument. *Geoscience and Remote Sensing, IEEE Transactions on*, *44*(5), 1093-1101. doi: 10.1109/TGRS.2006.872333

Livesey, N. J., Read, W. G., Wagner, P. A., Froidevaux, L., Lambert, A., Manney, G. L., ... Martinez, E. (2017). Version 4.2x level 2 data quality and description document. *JPL D-33509 Rev. C*. Retrieved from `https://mls.jpl.nasa.gov/data/v4-2\_data\_quality\_document.pdf`

Manney, G., Livesey, N. J., Santee, M. L., Froidevaux, L., Lambert, A., Lawrence, Z., ... Fuller, R. (2020). Record-low Arctic stratospheric ozone in 2020: MLS observations of chemical processes and comparisons with previous extreme winters. *Geophys. Res. Lett.*. (submitted)

Manney, G. L., Santee, M. L., Rex, M., Livesey, N. J., Pitts, M. C., Veefkind, P., ... Zinoviev, N. S. (2011). Unprecedented Arctic ozone loss in 2011. *Nature*, *478*, 469-475. doi: 10.1038/nature10556

McKenna, D. S., Grooß, J.-U., Günther, G., Konopka, P., Müller, R., Carver, G., & Sasano, Y. (2002). A new Chemical Lagrangian Model of the Stratosphere (CLaMS): 2. Formulation of chemistry scheme and initialization. *J. Geophys. Res.*, *107*(D15), 4256. doi: 10.1029/2000JD000113

Morcrette, J.-J. (1991). Radiation and cloud radiative properties in the European Centre for Medium-Range Weather Forecasts forecasting system. *J. Geophys. Res.*, *96*(D5), 9121-9132.

Müller, R., Crutzen, P. J., Grooß, J.-U., Brühl, C., Russell III, J. M., Gernandt, H., ... Tuck, A. F. (1997). Severe chemical ozone loss in the Arctic during the winter of 1995-96. *Nature*, *389*, 709-712.

Müller, R., Grooß, J.-U., Lemmen, C., Heinze, D., Dameris, M., & Bodeker, G. (2008). Simple measures of ozone depletion in the polar stratosphere. *Atmos. Chem. Phys.*, *8*(2), 251–264.

Müller, R., Grooß, J.-U., McKenna, D. S., Crutzen, P. J., Brühl, C., Russell, J. M., & Tuck, A. F. (1997). HALOE observations of the vertical structure of chemical ozone depletion in the Arctic vortex during winter and early spring 1996-1997. *Geophys. Res. Lett.*, *24*, 2717-2720.

Müller, R., Grooß, J.-U., Zafar, A. M., Robrecht, S., & Lehmann, R. (2018). The

maintenance of elevated active chlorine levels in the antarctic lower stratosphere through hcl null cycles. *Atmos. Chem. Phys.*, *18*(4), 2985–2997. doi: 10.5194/acp-18-2985-2018

Müller, R., Peter, T., Crutzen, P. J., Oelhaf, H., Adrian, G. P., v. Clarmann, T., ... Lary, D. (1994). Chlorine chemistry and the potential for ozone depletion in the Arctic stratosphere in the winter of 1991/92. *Geophys. Res. Lett.*, *21*, 1427-1430.

Nash, E. R., Newman, P. A., Rosenfield, J. E., & Schoeberl, M. R. (1996). An objective determination of the polar vortex using Ertel's potential vorticity. *J. Geophys. Res.*, *101*, 9471-9478.

Newman, P. A., Daniel, J. S., Waugh, D. W., & Nash, E. R. (2007). A new formulation of equivalent effective stratospheric chlorine (EESC). *Atmos. Chem. Phys.*, *7*(17), 4537–4552.

Newman, P. A., Gleason, F., McPeters, R., & Stolarski, R. (1997). Anomalously low ozone over the Arctic. *Geophys. Res. Lett.*, *24*, 2689-2692. doi: 10.1029/97GL52381

Pommereau, J.-P., Goutail, F., Lefèvre, F., Pazmino, A., Adams, C., Dorokhov, V., ... van Roozendael, M. (2013). Why unprecedented ozone loss in the Arctic in 2011? Is it related to climate change? *Atmos. Chem. Phys.*, *13*(10), 5299–5308. doi: 10.5194/acp-13-5299-2013

Pommereau, J.-P., Goutail, F., Pazmino, A., Lefvre, F., Chipperfield, M. P., Feng, W., ... Sitnikova, V. (2018). Recent arctic ozone depletion: Is there an impact of climate change? *Comptes Rendus Geoscience*, *350*, 347 - 353. (30th Anniversary of the Montreal Protocol: From the safeguard of the ozone layer to the protection of the Earth Climate) doi: 10.1016/j.crte.2018.07.009

Pommrich, R., Müller, R., Grooß, J.-U., Konopka, P., Ploeger, F., Vogel, B., ... Riese, M. (2014). Tropical troposphere to stratosphere transport of carbon monoxide and long-lived trace species in the Chemical Lagrangian Model of the Stratosphere (CLaMS). *Geosci. Model Dev.*, *7*(6), 2895–2916. Retrieved from `http://www.geosci-model-dev.net/7/2895/2014/` doi: 10.5194/gmd-7-2895-2014

Rex, M., Salawitch, R. J., Deckelmann, H., von der Gathen, P., Harris, N. R. P., Chipperfield, M. P., ... Zerefos, C. (2006). Arctic winter 2005: Implications for stratospheric ozone loss and climate change. *Geophys. Res. Lett.*, *33*. doi: 10.1029/2006GL026731

Rieder, H. E., & Polvani, L. M. (2013). Are recent Arctic ozone losses caused by increasing greenhouse gases? *Geophys. Res. Lett.*, *40*(16), 4437-4441. doi: {10.1002/grl.50835}

Rieder, H. E., Polvani, L. M., & Solomon, S. (2014). Distinguishing the impacts of ozone-depleting substances and well-mixed greenhouse gases on Arctic stratospheric ozone and temperature trends. *Geophys. Res. Lett.*, *41*(7), 2652-2660. doi: {10.1002/2014GL059367}

Solomon, S. (1999, August). Stratospheric ozone depletion: A review of concepts and history. *Rev. Geophys.*, *37*(3), 275-316. doi: 10.1029/1999RG900008

Solomon, S., Portmann, R. W., Sasaki, T., Hofmann, D. J., & Thompson, D. W. J. (2005). Four decades of ozonesonde measurements over Antarctica. *J. Geophys. Res.*, *110*(D21). doi: 10.1029/2005JD005917

Strahan, S. E., Douglass, A. R., Newman, P. A., & Steenrod, S. D. (2014). Inorganic chlorine variability in the Antarctic vortex and implications for ozone recovery. *J. Geophys. Res.*. doi: 10.1002/2014JD022295

Tilmes, S., Müller, R., Engel, A., Rex, M., & Russell III, J. (2006). Chemical ozone loss in the Arctic and Antarctic stratosphere between 1992 and 2005. *Geophys. Res. Lett.*, *33*. doi: 10.1029/2006GL026925

Tilmes, S., Müller, R., Grooß, J.-U., & Russell, J. M. (2004). Ozone loss and chlorine activation in the Arctic winters 1991–2003 derived with the

tracer-tracer correlations. *Atmos. Chem. Phys.*, *4*(8), 2181-2213. doi: 10.5194/acp-4-2181-2004

Tritscher, I., Grooß, J.-U., Spang, R., Pitts, M. P., Poole, L. R., Müller, R., & Riese, M. (2019). Lagrangian simulation of ice particles and resulting dehydration in the polar winter stratosphere. *Atmos. Chem. Phys.*, *19*, 543–563. doi: 10.5194/acp-19-543-2019

Weber, M., Dikty, S., Burrows, J., H. Garny, M. D., Kubin, A., Abalichin, J., & Langematz, U. (2011). The brewer-dobson circulation and total ozone from seasonal to decadal time scales. *Atmos. Chem. Phys.*, *11*(21), 11221-11235. doi: 10.5194/acp-11-11221-2011

Wegner, T., Pitts, M. C., Poole, L. R., Tritscher, I., Grooß, J.-U., & Nakajima, H. (2016). Vortex-wide chlorine activation by a mesoscale psc event in the arctic winter of 2009/10. *Atmos. Chem. Phys.*, *16*, 4569–4577. doi: 10.5194/acp-16-4569-2016

WMO. (2019). *Scientific assessment of ozone depletion: 2018*. Geneva, Switzerland: Global Ozone Research and Monitoring Project–Report No. 58.

Zhong, W., & Haigh, J. D. (1995). Improved broadband emissivity parameterization for water vapor cooling rate calculations. *J. Atmos. Sci.*, *52*(1), 124-138.

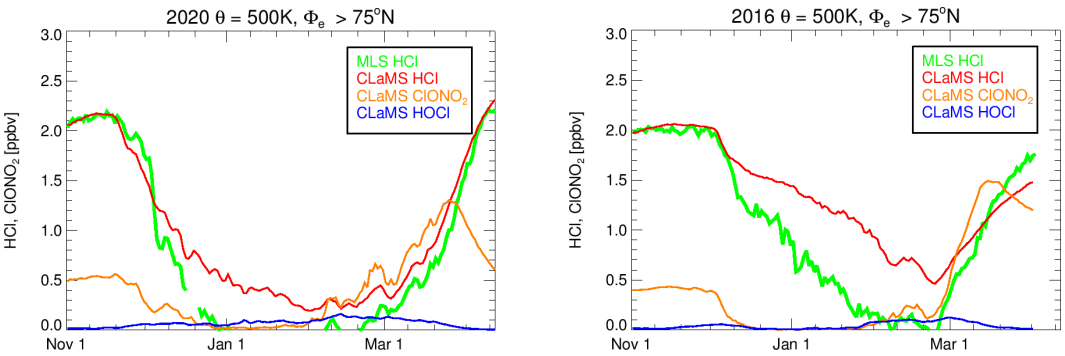

Figure 9. Vortex core average HCl, $ClONO_2$ and HOCl mixing ratios on the 500 K potential temperature level simulated by CLaMS and observed HCl by MLS. (a) Current simulation for 2019/2020 and (b) simulation for 2015/2016 by Grooß et al. (2018).